Smaller is Faster and More Sensitive: The Effect of Wire Size on the Detection of Hydrogen by Single Palladium Nanowires

Fan Yang, Sheng-Chin Kung, Ming Cheng, John C. Hemminger, and Reginald M. Penner*

Department of Chemistry, University of California, Irvine, California 92697-2025

ABSTRACT Palladium nanowires prepared using the lithographically patterned nanowire electrodeposition (LPNE) method are used to detect hydrogen gas (H_2). These palladium nanowires are prepared by electrodepositing palladium from EDTA-containing solutions under conditions favoring the formation of β-phase PdH_x. The Pd nanowires produced by this procedure are characterized by X-ray diffraction, transmission electron microscopy, scanning electron microscopy, atomic force microscopy, and X-ray photoelectron spectroscopy. These nanowires have a mean grain diameter of 15 nm and are composed of pure Pd with no XPS-detectable bulk carbon. The four-point resistance of 50−100 μm segments of individual nanowires is used to detect H_2 in N_2 and air at concentrations ranging from 2 ppm to 10%. For low $[H_2] < 1\%$, the response amplitude increases by a factor of 2−3 with a reduction in the lateral dimensions of the nanowire. Smaller nanowires show accelerated response and recovery rates at all H_2 concentrations from, 5 ppm to 10%. For 12 devices, response and recovery times are correlated with the surface area/volume ratio of the palladium detection element. We conclude that the kinetics of hydrogen adsorption limits the observed response rate seen for the nanowire, and that hydrogen desorption from the nanowire limits the observed recovery rate; proton diffusion within PdH_x does not limit the rates of either of these processes.

KEYWORDS: hydrogen · sensor · electrodeposition · palladium · hydride

Although it has been known for more than 100 years that the absorption of hydrogen by palladium hydride, PdH_x, increases its electrical resistivity,[1] it was not until 1992 that Hughes and Schubert[2] demonstrated that palladium alloy resistors consisting of ultrathin palladium−nickel alloy films could be used as H_2 sensors. In that work, Pd−Ni(8−20%) films with thicknesses in the 50 nm range produced response times of ~10 s at 4% H_2 and ~20 s at 1% H_2 while achieving a limit of detection (LOD_{H_2}) below 0.1%.[2] The presence of nickel in the palladium sensing element suppresses the α- to β-phase transition that is responsible, in pure palladium films, for irreproducibility and hysteresis in the detection of hydrogen at concentrations above 1% H_2 (at 300 K). The Pd−Ni thin film resistor achieves many design objectives for hydrogen safety sensors including a low manufacturing cost, high sensitivity and accuracy, good stability, and a simple, rugged design, but its response times (10−20 s) are too slow by approximately an order of magnitude, based upon recent Department of Energy mandated performance metrics.[3]

Several innovative resistive sensor designs have improved upon the response time of the Hughes thin film sensor at the expense of additional device complexity. For example, Wang and co-workers[4] prepared hydrogen-sensitive resistors by decorating nanoporous alumina surfaces with palladium nanoparticles. The resulting devices produced a response at 1% H_2 of ~1 s and a LOD_{H_2} of 500 ppm.[4] Dimeo *et al.*[5] described a MEMS-based hydrogen sensor in which thin films of a rare earth were employed as resistors on a microfabricated silicon platform[6] that facilitated the heating of these films to 50− 80 °C. This device produced response times of 0.5 s and a LOD_{H_2} of less than 200 ppm.[5]

A distinct subcategory of resistive hydrogen sensors involves ultrathin palladium film resistors that operate at the percolation threshold for electrical conduction. These sensors transduce the presence of hydrogen as a resistance *decrease* ($\Delta R_{H_2} < 0$), in contrast to the resistance increase ($\Delta R_{H_2} > 0$) normally seen for palladium resistors. Decreased resistance within the film is induced by volumetric swelling of β-phase PdH_x by 10% as compared with the α-phase,[1] opening new electrical pathways for transport within the film. Kaltenpoth *et al.*[7] were the first to observe this mechanism in ultrathin palladium films prepared within microfabricated silicon channels, but the performance of these devices was

*Address correspondence to rmpenner@uci.edu.

Received for review June 29, 2010 and accepted July 30, 2010.

Published online August 13, 2010. 10.1021/nn101475c

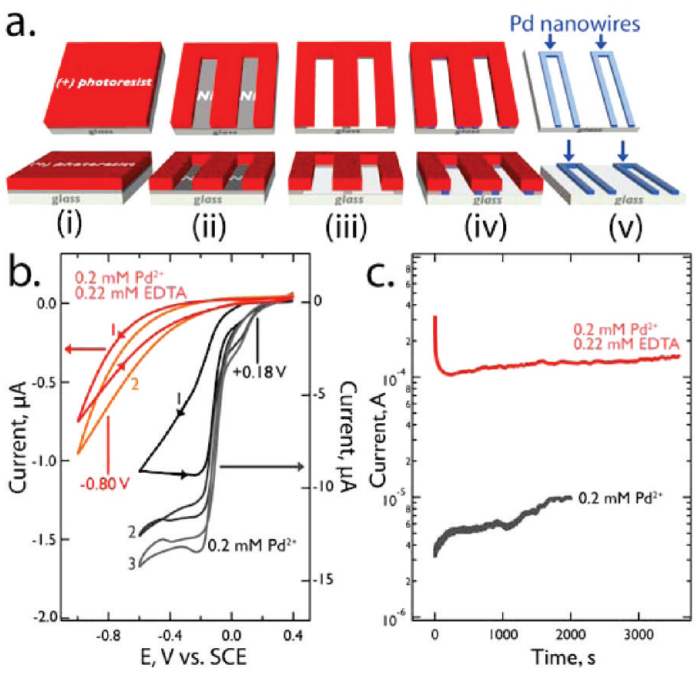

Figure 1. Fabrication of palladium nanowires using the LPNE method. (a) Nickel layer is evaporated onto a glass surface and covered with a layer of photoresist (step i). The PR layer is photopatterned using a contact mask (step ii), and the exposed nickel is etched in nitric acid to produce a horizontal trench along the perimeter of the exposed region (step iii). A Pd nanowire is electrodeposited into this horizontal trench (step iv). The photoresist and remaining nickel are removed using acetone and nitric acid, respectively (step v). (b) Cyclic voltammograms of a Pd plating solution containing 0.2 mM Pd^{2+} (black and gray) and a Pd plating solution containing 0.2 mM Pd^{2+} and 0.22 mM ethylenediamine tetraacetic acid (EDTA, red and orange) showing the potentials used for potentiostatic Pd deposition. Both of these CVs were obtained at microfabricated nickel edges with 60 nm height. (c) Current *versus* time for the potentiostatic electrodeposition of Pd nanowires, both of which had a final thickness and width of 20 nm × 150 nm and identical length, within an LPNE template using the same two solutions and deposition potentials indicated in (b).

improved upon by Xu *et al.*,[8] who used palladium island films evaporated onto glass surfaces modified with a siloxane self-assembled monolayer as the resistive sensing element. Their "monolayer enhanced" sensors achieved a response time of 70 ms at 2% and a LOD_{H_2} of 25 ppm.[8] A systematic study of this hydrogen detection mode by Ramanathan *et al.*[9] concluded, however, that an extremely narrow range of palladium coverages, corresponding to palladium layer thickness of 2−3 nm, are required in order to obtain this hydrogen sensing response.

Resistive sensors based upon palladium nanowires retain the simplicity of Hughes' palladium film resistors while offering the possibility for accelerated sensor response and recovery. Work in this direction dates to 2000 when we[10] reported an investigation of the properties of ~200 nm diameter palladium nanowires for detecting H_2 and found that these nanowires spontaneously fractured upon exposure to H_2 above 1−2%. Such fractured nanowire ensembles were nevertheless able to detect hydrogen gas because, like the percolation-based sensors described above, swelling of β-phase PdH_x grains mechanically closes these fractures, causing the resistance of Pd nanowire ensembles to decrease in the presence of hydrogen above 1−2%.[10] This LOD_{H_2} is, of course, much too high for safety sensors given that the lower explosion limit for H_2 in air is 4%.[3] More recently, microfabricated versions of this "fractured-wire" device[11,12] have been described. Since 2000, we[12−16] and others[11,14,17−20] have studied single palladium nanowire sensors with an eye to improving both LOD_{H_2} and the temporal properties of H_2 detection, and progress has been made on both fronts. For example, both Offermans *et al.*[20] and Yang *et al.*[12,15] have reported LOD_{H_2} in the low parts per million range and response/recovery times of a few seconds at H_2 concentrations of a few percent using Pd nanowires that do not fracture upon exposure to H_2, even at high concentrations.

In this paper, we examine the influence of the lateral wire dimensions on the function of single nanowire hydrogen sensors. Our conclusions are based on an examination of data for 14 hydrogen sensors: 11 single palladium nanowire sensors and three palladium film resistors. The nanowires in these devices were prepared using the lithographically patterned nanowire electrodeposition (LPNE) method.[21−23] LPNE produces palladium nanowires with a rectangular cross section having well-defined thickness (defined here as the wire dimension perpendicular to the surface) and width. In preliminary work,[12] we discovered that the addition of EDTA to the Pd plating solution produced nanowires that did not fracture during exposure to hydrogen, whereas in the absence of EDTA, wire fracture occurred in virtually every device.[10,12,13] Here, we undertake the chemical characterization of these nanowires by XPS depth profiling in order to ascertain whether carbon incorporation into the palladium lattice occurs during wire growth from these solutions. The thickness of the three palladium films (of 11, 22, and 49(±1) nm) was selected to match that of nine nanowires, allowing us to make a direct comparison of films to nanowires in terms of their respective H_2 sensing performance. We also compare the properties of nanowires for detecting hydrogen in air and nitrogen backgrounds for two nanowire-based devices. Data compiled for these 14 sensors, coupled with recent experiments in which the temperature dependence of the sensing behavior has been probed,[15] provide a basis for identifying the chemical processes that are rate-limiting in terms of the response and recovery of Pd nanowires to hydrogen.

RESULTS AND DISCUSSION

Palladium Nanowire Fabrication and Characterization. The LPNE method involves the fabrication of a temporary, sacrificial template on a glass or oxidized silicon surface (Figure 1).[21,22] This template is formed by first vapor depositing a nickel layer with a thickness of 5−100 nm, covering the nickel layer with a photoresist (PR), photo-

patterning the PR layer using a contact mask, and then removing the exposed nickel using nitric acid. The nickel layer is intentionally "over etched" so that the PR layer is undercut by approximately 300−500 nm (Figure 1a, iv) at the perimeter of the exposed region. This undercut produces a horizontal trench along the entire perimeter of the patterned region. A nanowire is formed within this trench by electrodeposition: The template is first immersed into an aqueous plating solution, and nanowires of the desired composition and width are produced by electrodeposition using the nickel edge within the trench as a working electrode. Finally, the template, consisting of the PR and nickel layers, is removed by dissolution in acetone and nitric acid, respectively, to expose the electrodeposited nanowires (Figure 1a, v). Useful features of the LPNE method include the following: (1) the position and two-dimensional trajectory of nanowires on the glass surface are controlled using photolithography; (2) the nanowire thicknesses, perpendicular to the surface, is determined by the thickness of the evaporated nickel layer; and (3) the nanowire width is determined by the electrodeposition parameters including the applied voltage, the solution composition, and the deposition duration.

The nanowire-based hydrogen sensors studied in this paper were all produced from palladium plating solutions containing a slight stoichiometric excess of ethylenediamine tetraacetic acid (EDTA, aq 0.2 mM $PdCl_2$, 0.22 mM EDTA). Previously, EDTA has often been used to modify the morphology of electrodeposited metal films.[24−26] In earlier work,[12] we discovered that the Pd nanowires deposited from solutions containing EDTA (henceforth, "+EDTA" nanowires) are resistant to fracture upon exposure to high concentrations of H_2, whereas "−EDTA" nanowires, grown from EDTA-free plating solutions, consistently fractured upon exposure to H_2 above 2%. We did not speculate on the origin of this increased toughness of +EDTA nanowires earlier, and the origin of this disparate behavior remains under investigation in our laboratory. Additional information pertaining to the structure and chemical composition of both types of nanowires is disclosed here. On the basis of these data, our hypothesis is that, in the presence of EDTA, β-phase PdH_x, not palladium metal, is the product of the electrodeposition reaction. This hypothesis is supported by electrochemical data: The voltammetry of an LPNE-templated nickel electrode in this solution (Figure 1b) and in an identical solution without EDTA reveal that, in the EDTA solution, the onset for palladium deposition is shifted to more negative potentials by ~500 mV, just as expected for strong complexation of the Pd^{2+} by EDTA. In the absence of EDTA at 0.18 V *vs* SCE, Pd deposition occurs with high current efficiency:

$$Pd^{2+}(aq) + 2e^- \rightarrow Pd(s) \qquad (1)$$

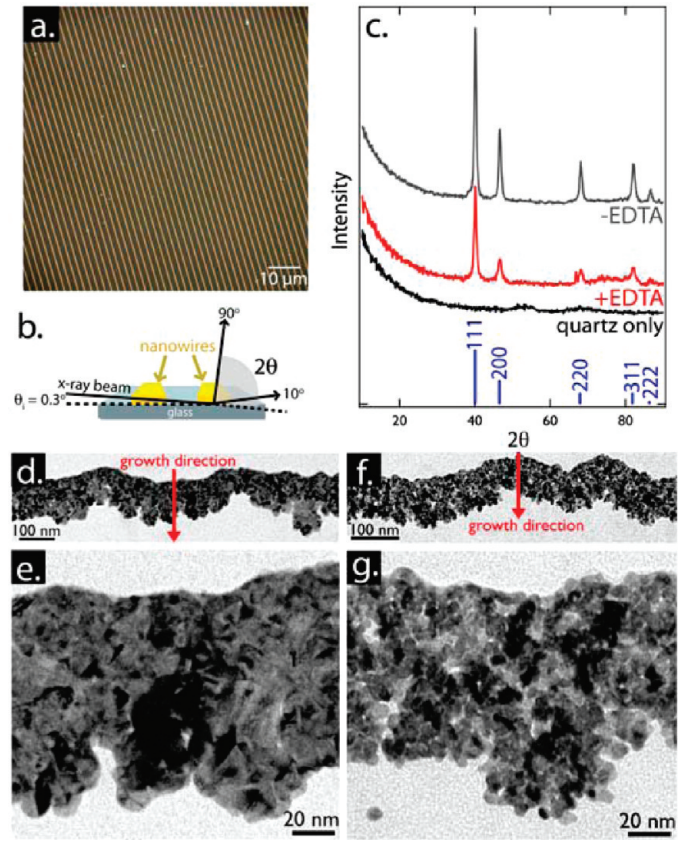

Figure 2. Characterization of Pd nanowires using X-ray diffraction (XRD) and transmission electron microscopy (TEM). (a) Optical micrograph showing an array of Pd nanowires deposited at 2 μm pitch on quartz. Samples like this one were used to acquire data for XRD and X-ray photoelectron spectroscopy (XPS). (b) XRD data were acquired using grazing incidence with a fixed incident angle of 0.3°. (c) XRD patterns for Pd nanowires prepared from plating solutions that either contained added EDTA (+EDTA; aq 0.2 mM $PdCl_2$, 0.22 mM EDTA) or without added EDTA (−EDTA; aq 0.2 mM $PdCl_2$); (d,e) TEM images at low and high magnification, respectively, of +EDTA Pd nanowires, and (f,g) TEM images of −EDTA Pd nanowires.

The current plateau seen at negative potentials in the EDTA-free plating solution affords an estimate of the Pd^{2+} diffusion-controlled current of 10−12 μA. In the EDTA-containing solution, deposition at −0.80 V *vs* SCE produces a total current of 100−110 μA for an identical LPNE-templated electrode—larger than the Pd^{2+} diffusion-controlled current by a factor of about 10. The two nanowires prepared in the experiments of Figure 1c were both 20 × 150 nm in lateral dimensions (henceforth: height × width), so the additional deposition charge (Q_{+EDTA} = 0.465 C *versus* Q_{-EDTA} = 0.132 C) is not explained by the deposition of additional Pd. Instead, the larger deposition current seen in the EDTA solution is produced by the availability at these more negative potentials of two new reactions in addition to Pd^{2+} deposition:

$$H^+(aq) + e^- \rightarrow H_2(g) \qquad (2)$$

$$xH^+(aq) + xe^- + Pd(s) \rightarrow PdH_x(s) \qquad (3)$$

Both of these reactions can contribute to the formation

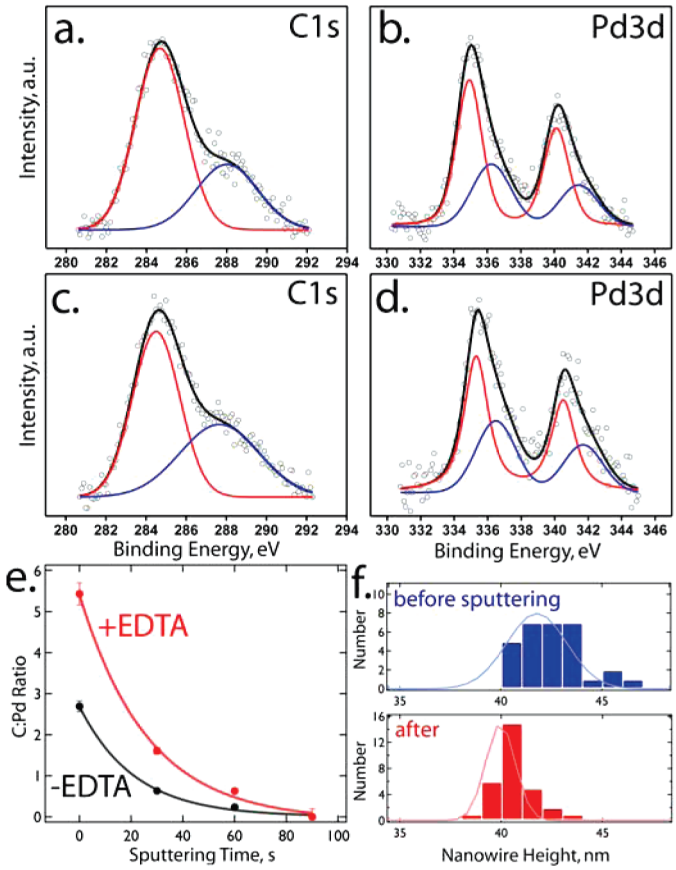

Figure 3. X-ray photoelectron spectroscopy (XPS) analysis of +EDTA and −EDTA palladium nanowires: (a,b) C1s and Pd3d scans, respectively, of −EDTA Pd nanowires. (c,d) C1s and Pd3d scans, respectively, of +EDTA Pd nanowires. (e) Plot of the ratio between the integrated C1s signal and the integrated Pd3d signal as a function of sputtering time for +EDTA nanowires (red) and −EDTA nanowires (black). Excess EDTA-derived carbon is observed by XPS within the first 2 nm of the surface. (f) Atomic force microscopy height histograms for +EDTA nanowires before (top) and after (bottom) 90 s of Ar^+ sputtering at 2 keV and 20 mA. A total of 2−3 nm of Pd is removed by this process.

of β-phase PdH_x. The PdH_x formed by electrodeposition in EDTA solution will spontaneously convert to Pd metal as soon as the potentiostat releases the nanowires to open-circuit, and the +EDTA nanowires are exposed to air, but these nanowires will retain a "built-in" tensile stress because the β-phase PdH_x has a volume 10% larger than that of Pd metal. It is possible, but still unproven, that this residual tensile stress counteracts the compressive stress that is imposed upon exposure of Pd nanowires to $[H_2]$ above 2% and the formation of β-phase PdH_x—a process that reproducibly fractures the −EDTA Pd nanowires.

+EDTA and −EDTA nanowires are remarkably similar in terms of their microstructure and grain diameter (Figure 2). Grazing incidence X-ray diffraction analysis (Figure 2a,b) shows that both types of nanowires are single phase, fcc Pd (JCPDS 01-088-2335). GIXRD permits the out-of-plane grain diameter, $D_\perp$, to be estimated from the X-ray line widths using the Scherrer equation, $D_\perp = 0.89(\lambda)/(B \cos \theta)$. For +EDTA and −EDTA nanowires, we measure virtually identical $D_\perp$ values of 12 ± 1 and 14 ± 1 nm, respectively. Transmission electron microscopy (TEM) can be used to visualize the in-plane grain dimension for these same nanowires,[12] and these $D_\parallel$ values are 15 ± 1 and 6 ± 3 nm for +EDTA and −EDTA nanowires, respectively.[12] Thus, both +EDTA and −EDTA nanowires are phase-pure fcc palladium with similar nanoscopic grain dimensions.

The presence of EDTA-derived carbon within the deposited palladium can be ruled out by X-ray photoelectron spectroscopy (XPS) analysis (Figure 3). In the C1s spectral region, two chemical states, characterized by binding energies of 284 and 288 eV, are observed. The lower binding energy component is characteristic of saturated hydrocarbon, and the higher binding energy is typical of oxidized carbon moieties such as carbonate and acetate.[27] The Pd3d region also shows the presence of two chemical states for palladium with $3d_{5/2}$ binding energies of 334 and 336.5 eV. The lower energy peak is characteristic of Pd^0, whereas the higher binding energy component is likely caused by the presence on the surface of PdO.[27] Except for the ratio between the total carbon and palladium, the surfaces of +EDTA and −EDTA nanowires are chemically indistinguishable by XPS. The "bulk" composition of these nanowires were probed by XPS depth profiling analysis. In this case, we plot the ratio between the total carbon and the total palladium signal (C/Pd) in Figure 3e. The thickness of these nanowires, measured before and after this experiment, were reduced by just 2−3 nm over 90 s of total sputtering time. The initial C/Pd ratio measured for +EDTA nanowires is significantly higher than that observed for the −EDTA nanowires, consistent with the presence of adsorbed EDTA on the surfaces of the +EDTA nanowires, but the C/Pd ratio converges on 0 for both types of nanowires as Ar^+ sputtering proceeds. We conclude that carbon is not codeposited with palladium to any significant extent.

Collectively, the XRD, XPS, and TEM data of Figures 2 and 3 show that EDTA does not exert a strong influence on the structure and chemical composition of these electrodeposited Pd nanowires, and the reason for the additional fracture toughness of the +EDTA nanowires[12] is not apparent from these data. The electrochemical data of Figure 1, on the other hand, suggest that β-phase PdH_x may be deposited and, as already discussed above, the mechanical properties of the resulting nanowire should be affected. We have not yet obtained any direct confirmation for the formation in the EDTA-containing solution of β-phase PdH_x.

Detection of Hydrogen. The properties of +EDTA palladium nanowires for the detection of hydrogen (Figure 4, bottom) were compared to one another as a function of their thickness and width. The performance of these nanowires was also compared to palladium films ~100 μm in width (Figure 4, top) with thicknesses that matched those of the nanowires.

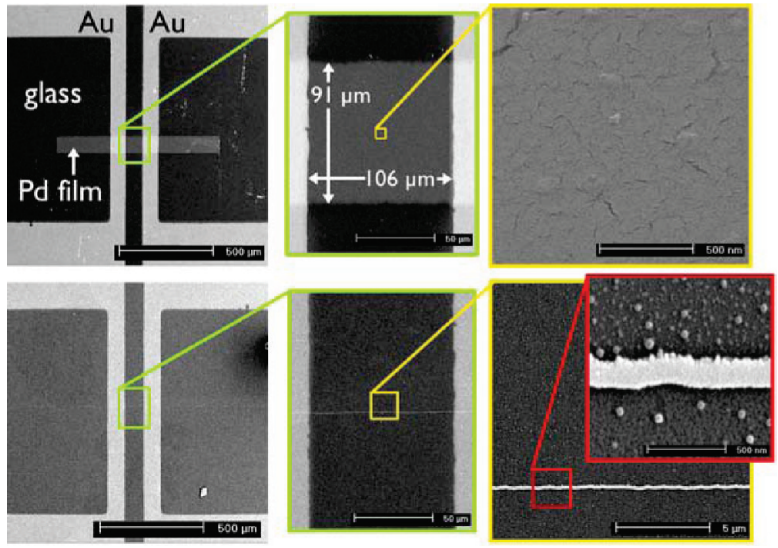

Figure 4. Two types of hydrogen sensors compared in this work. Top: Palladium film sensors consisting of a vapor-deposited palladium film of defined thickness that is 90−100 μm in total width. Gold electrical contacts are vapor-deposited at approximately 100 μm. Bottom: Palladium nanowire sensor consisting of a single, linear palladium nanowire of defined thickness and width with two evaporated gold contacts at either 50 or 100 μm.

The objectives of these comparisons are to (1) determine whether nanowires of a particular thickness have different properties for the detection of hydrogen as compared to Pd films of the same thickness, (2) investigate how the nanowire thickness and width influence the sensitivity to hydrogen as well as the temporal response properties, and (3) determine the rate-limiting processes that determine the response/recovery time for these devices.

The resistance change ratio, $\Delta R/R_0$, is plotted *versus* time in Figure 5 for three devices for which the Pd sensing element has a thickness in the 11−14 nm range. It is important, first of all, to recognize that all three devices successfully measure the presence of hydrogen as an increased resistance, which is qualitatively as expected since PdH_x has a bulk resistance that is higher compared to that of Pd^0 by up to a factor of 1.8 (for $x = 0.7$).[1] This factor of 1.8 should translate into a $\Delta R/R_0$ value at sufficiently high H_2 concentration of 80%, but the largest $\Delta R/R_0$ values observed for these devices (Figure 5d) are in the 18−20% range. This maximum resistance change value is, nevertheless, somewhat higher than seen previously for Pd ultrathin films and nanowires by other research groups. For example, Hughes *et al.*[2] reported a maximum $\Delta R/R_0$ of ~9% for Pd/Ni(8%) films and ~8% for Pd/Ni(15%) films. Offermans *et al.*[20] reported $\Delta R/R_0$ of ~14% for single 50−80 nm Pd nanowires, and Rumiche *et al.*[4] reported $\Delta R/R_0$ ranging from 0.5 to 3% at $[H_2] = 1\%$ for Pd nanowire arrays (for comparison, $\Delta R/R_0$ at $[H_2] = 1\%$ for the two nanowire devices screened in Figure 5 is 10−12%). It is also apparent that all three devices function over the entire H_2 concentration range from 200 ppm to 10%. In fact, the limit of detection (LOD_{H_2}) for hydrogen is always well

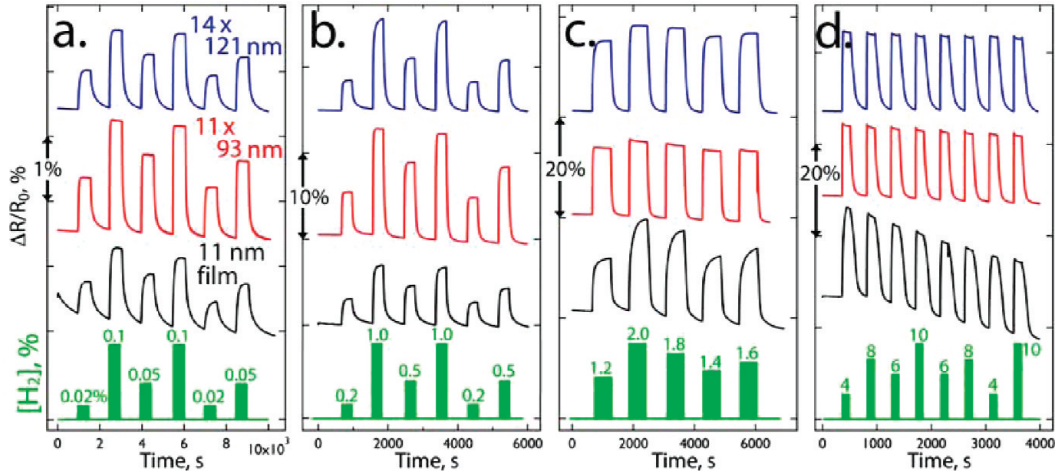

Figure 5. Raw hydrogen sensing data for three devices having a similar palladium thickness: a 14 × 121 nm nanowire, a 11 × 93 nm nanowire, and a 11 nm ×100 μm film. The hydrogen concentration program is plotted in green at the bottom of each data set (a−d).

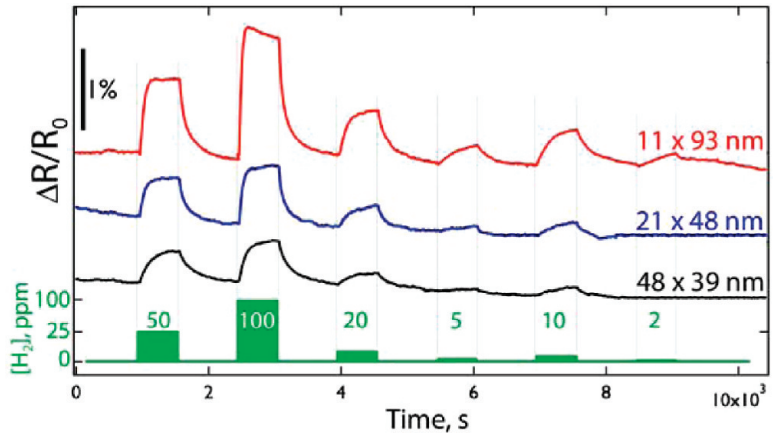

Figure 6. Resistance change ratio (R/R_0) *versus* time data for three single nanowire hydrogen sensors with the indicated lateral dimensions for 2 ppm ≥ [H_2] ≥ 100 ppm.

below 200 ppm (Figure 6) and varies from 2 to 100 ppm depending on the device. Beyond these similarities, one immediately observes systematic differences from device to device in terms of the sensitivity to hydrogen, the response time, and the recovery time. Specifically, the 11 × 93 nm nanowire is faster, in both response and recovery, and more sensitive than the 14 × 121 nm nanowire, which in turn is faster and more sensitive than the 11 nm film. Moreover, drift of the resistance baseline is pronounced for the 10 nm film at both high and low H_2 concentrations, but far less so for the two nanowires. Are these trends maintained over a larger number of devices? We examine first the issue of sensor sensitivity.

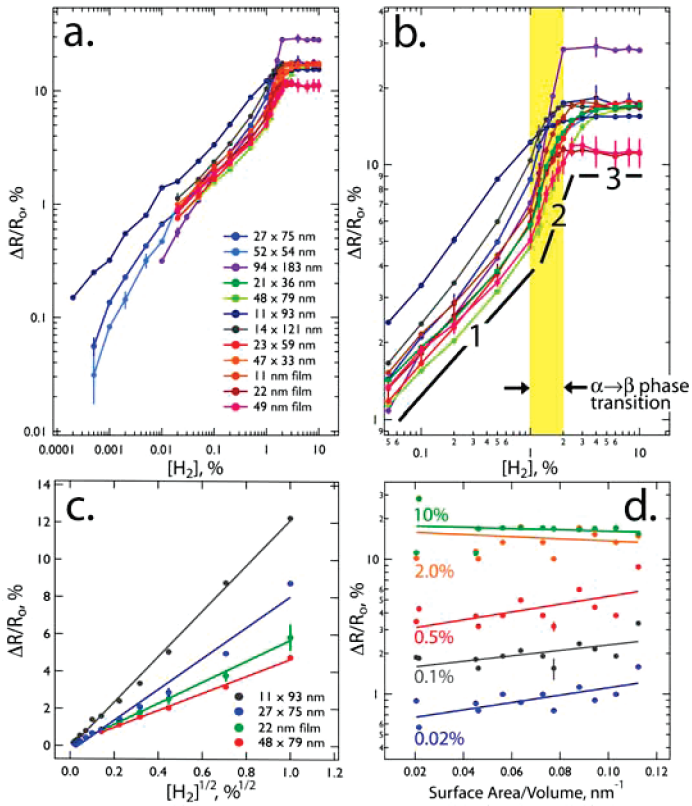

Figure 7. Sensitivity of Pd nanowire and film-based sensors to H_2. (a,b) Plots of $\Delta R/R_0$ *versus* [H_2] for nine Pd nanowire sensors and three evaporated Pd films, as indicated. (b) Three discrete response regimes, characterized by different sensitivities to H_2, can be distinguished in these data: Regime 1: For [H_2] ranging from very low concentrations to ~1%, $\Delta R/R_0$ is approximately proportional to $\sqrt{[H_2]}$, as shown in (c). Regime 2: For 1% < [H_2] < 2%, the sensitivity to H_2 is increased by up to a factor of 2 as compared with that seen at lower [H_2]. Regime 3: For [H_2] > 2%, $\Delta R/R_0$ is invariant. (d) Plots of $\Delta R/R_0$ *versus* surface area/volume ratio for five [H_2] as indicated. The sensitivity of α-phase PdH_x nanowires and nanofilms ([H_2] = 0.02, 0.1, 0.5%) to H_2 is increased slightly with increasing surface area/volume, whereas β-phase PdH_x wires and films ([H_2] = 2 and 10%) show no detectable effect. Error bars, representing ±1σ for multiple measurements, are shown only for S/A = 0.08 for clarity.

$\Delta R/R_0$ *versus* [H_2] calibration plots for 12 devices, including three films, are compared in Figure 7a,b. Three response regimes can be distinguished as a function of [H_2] in these plots (Figure 7b): For [H_2] < 1% (regime 1), $\Delta R/R_0$ increases in proportion to $\sqrt{[H_2]}$ (Figure 7c). In this [H_2] range, the sensing element is converted between Pd^0 and α-PdH_x ($x < 0.015$).[1] At higher [H_2] in the range from 1 to 2% (regime 2), the sensitivity is increased by approximately a factor of 2 for all devices. Across this concentration range, α-PdH_x is converted into β-PdH_x,[1] so a palladium sensing element is converted between Pd^0 and the α/β coexistence region of the PdH_x phase diagram.[1] For [H_2] > 2% (regime 3), the sensitivity falls abruptly to 0 (Figure 7b); no further change in $\Delta R/R_0$ is observed above 2% H_2 for either nanowires or films (Figure 5d). In this regime, the sensing element is converted between Pd^0 and β-PdH_x ($0.015 < x < 0.7$).[1] These three sensing regimes can be delineated in the data for all 14 devices studied in connection with this paper.

The $\Delta R/R_0 \propto \sqrt{[H_2]}$ behavior seen in regime 1 (Figure 7c) has been observed for the detection of [H_2] below 1% for a variety of Pd resistor-based hydrogen sensors[28,29] including those employing Pd nanowires.[4,20] An explanation for this behavior starts with Sievert's Law which postulates that the equilibrium constant for the reaction:

$$0.5H_2(gas) \rightarrow H(ads) \quad (4)$$

given by the expression, $K = (\sqrt{P_{H_2}})/(x_s)$ for small values of x_s, the H/Pd ratio in the bulk metal adjacent to the surface.[30] If we can assume that $x_s \approx x$, then eq 4 applies within α-PdH_x where $x < 0.015$. It is also well-established[31,32] that the electrical resistivity, ρ, of PdH_x within the α phase is directly proportional to x over a wide temperature range. Consequently, in regime 1, $\rho \propto \sqrt{P_{H_2}}$, as shown for four devices in Figure 7c, and the slope of this proportionality is positively correlated with the surface area/volume ratio of the sensing element (Figure 7d). Specifically, the slope of the $\Delta R/R_0$ *versus* surface area:volume ratio has a positive slope for all three α-phase concentrations of 0.02, 0.1, and 0.5%. This means that smaller nanowires have a higher resistance sensitivity to H_2 at low $[H_2]$, but this effect is modest with the sensitivity increasing by less than a factor of 2 over the range from $[H_2] = 0.02$ to 1%.

In regime 2, an increase in the sensitivity from regime 1 is observed for all devices (Figure 7b), and this has also been observed for Pd films[33] and nanowires.[4,20] The proportionality between ρ and x that characterizes the α-PdH_x is unchanged in this regime,[31,32] but within this narrow concentration interval, between 1 and 2% H_2, x increases from 0.015 to 0.60 because the α- to β-phase transition occurs. This Δx of 0.585 is larger by a factor of 39 compared with the total Δx of 0.015 seen over regime 1, and one projects an increased sensitivity directly proportional to this factor, but instead the $\Delta R/R_0$ increases by just a factor of 2−3 (also as seen previously for other devices[4,20,31,32]). The question is: why isn't the increase in sensitivity larger? Our speculation is that the phase transition, which induces a 3% increase in the lattice constant, mechanically compresses the nanowire along its axis, plastically deforming it and increasing its diameter slightly. If this compressive deformation occurs, the increased lateral dimensions of the nanowire would partially offset the increased resistance of the hydride, leading to a maximum $\Delta R/R_0$ lower than 80%, qualitatively as observed, but this hypothesis is unproven at present.

Regime 3 is characterized by a $\Delta R/R_0$ response that is virtually independent of $[H_2]$ for all 12 devices (Figure 7b). This behavior is unique to our devices; it has not been reported for other Pd nanowire or film sensors, to our knowledge, and the origin for this response has not been resolved. It is worth noting, however, that the "saturation" of $\Delta R/R_0$ signal above $[H_2] = 2\%$ is observed both for our electrodeposited nanowires and for the three devices based on evaporated Pd films (Figure 7b). For other resistance sensors derived from Pd films[31−33] and nanowires,[4,20] the resistance continues to increase with $[H_2]$ in this regime. The proportionality between ρ and x is unchanged at these high H_2 concentrations,[31,32] but the rate of change for x with $[H_2]$ is close to the values seen for α-PdH_x in regime 1. It is possible, but unconfirmed, that the mechanical stress effect discussed in the preceding paragraph offsets the resistance increase caused by an increase in x in this concentration range. This loss of sensitivity for $[H_2] > 2\%$ is certainly a deficiency of our device because the precision of the $[H_2]$ measurement is compromised at these high $[H_2]$, but the functionality of the device as a H_2 safety sensor is unaffected since this application requires only that the sensor signal the presence of H_2 above a critical concentration.

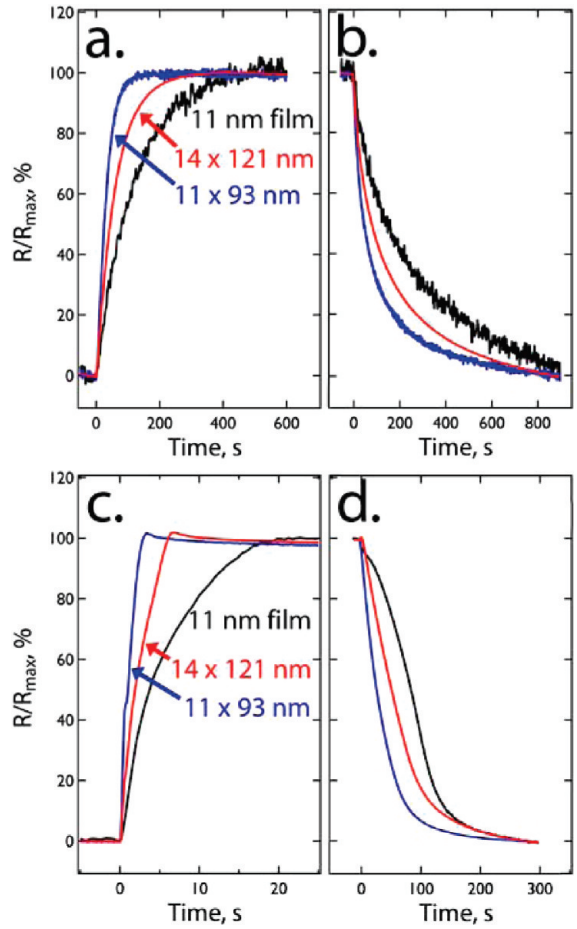

Figure 8. Normalized resistance, R/R_{max}, *versus* time for the response (a,c) and recovery (b,d) for three devices having a similar palladium thickness: a 14 × 121 nm nanowire, a 11 × 93 nm nanowire, and a 11 nm ×100 μm film. Data for two $[H_2]$ are shown: $[H_2] = 0.020\%$ (a,b) and $[H_2] = 10.0\%$ (c,d).

We now discuss the rate at which these sensors respond to, and recover from, H_2 exposure. Normalized R/R_{max} *versus* time plots for three devices (Figure 8) show significant differences in spite of the fact that the smallest lateral dimensions for these three sensors—the thickness—are similar ranging from 11 to 14 nm. This thickness dimension is the minimum distance over which the diffusion of protons in PdH_x must occur during the equilibration of the sensing

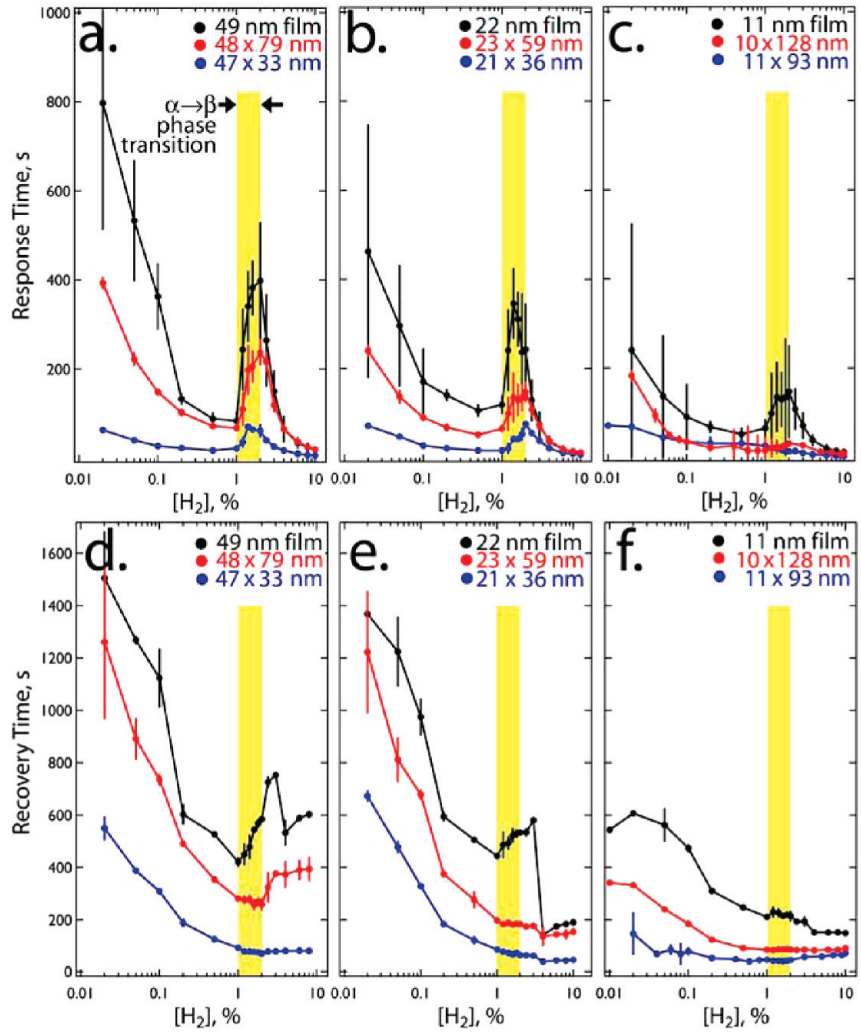

Figure 9. Plots of response time (a−c) and recovery time (d−f) for three sets of devices having the same (or similar) thickness and different widths. Each set of devices include an evaporated Pd film with a width of 100 μm: (a,d) 49 nm film, 48 × 79 nm nanowire, 47 × 33 nm nanowire; (b,e) 22 nm film, 23 × 59 nm nanowire, 21 × 36 nm nanowire; (c,f) 11 nm film, 10 × 128 nm nanowire, 11 × 93 nm nanowire.

element with H_2. Response and recovery were tested at two concentrations, $[H_2] = 0.02$ and 10%, below and above the α- to β-phase transition. From these data, a response time is defined as the time necessary for the resistance to increase from R_0, the equilibrium value in pure N_2, to $0.90R_{max}$ while the recovery time is the analogous quantity for the reverse process. In the case of the 11−14 nm devices (Figure 9a), nanowires are faster than films of the same thickness. The same conclusion holds up for devices with matched thicknesses of ~22 and ~48 nm (Figure 9b,c). Collectively, these data support the conclusion that diffusion across the smallest dimension of these structures does not limit response and recovery rates. Of course, if proton diffusion limits both response and recovery, then one would expect the rates of these two processes to be similar, whereas the data of Figure 9 show that recovery is slower than response by a factor of 2 or more.

The observed insensitivity to diffusion seen here stands in contrast to earlier measurements of the reaction rate of hydrogen on single-crystalline palladium films that were 0.88 mm in total thickness by Goodman *et al.*[34] In that work, a proton diffusion-controlled adsorption rate for hydrogen was observed. The key difference between our experiment and that of Goodman *et al.* is the diminutive thickness of the nanowires and films probed here as compared with those studied earlier. The importance of the thickness difference can be appreciated from the following calculation: Einstein's expression for the root-mean-square displacement, x, of a diffuser as a function of time, t, $x = \sqrt{2Dt}$ can be evaluated using the measured diffusion coefficient, D_H, for H in nanocrystalline (grain diameter ≈ 5 nm) α-PdH_x at room temperature, $D_H = 5 \times 10^{-8}$ cm^2/s[35] and $x =$ 48 nm. Solving for time, one obtains $t = 2.3 \times 10^{-4}$ s, 3−5 orders of magnitude smaller than the re-

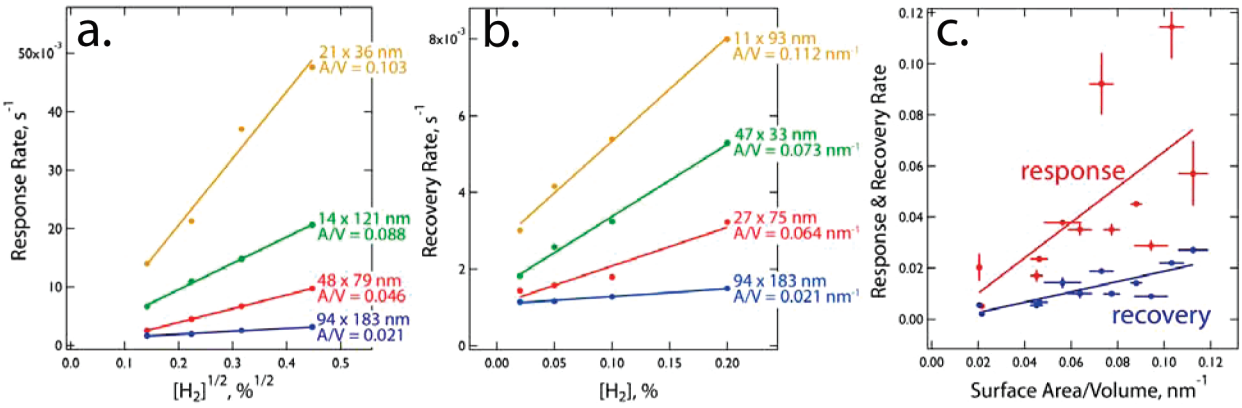

Figure 10. (a) Plots of response rate *versus* $\sqrt{[H_2]}$ for four nanowires, with the indicated dimensions, at $[H_2] < 1\%$. (b) Plots of recovery rate *versus* $[H_2]$ for four nanowires, with the indicated dimensions, at $[H_2] < 1\%$. (c) Plot of the slopes of the two relationships evaluated in (a) and (b) *versus* the surface area/volume ratio (SA/*V*) for 12 sensors.

sponse and recovery times measured for these nanowires at room temperature (Figure 9a,d). If the thickness of the palladium sample is increased to 0.88 mm, a factor of $>10^4$, the time required for equilibration increases by $>10^8$ to more than 20 h, fully accounting for the diverging conclusions of our two studies.[34]

If diffusion does not limit the response and recovery rates for these devices, then what process does? Recently,[15] we examined the temperature dependence of the response and recovery rates for single nanowire sensors in flowing N_2. The measured activation energies, E_a, supported the conclusion that H_2 adsorption limits the response rate of these sensors for $[H_2] < \sim 1\%$ (*i.e.*, α-PdH_x) and that at higher H_2 concentrations, where β-PdH_x is formed, a higher activation energy is measured that corresponds to the α- to β-phase transition. Measured E_a values for recovery were consistent with the complementary process, H_2 desorption from palladium, again for low $[H_2] < \sim 1\%$ (*i.e.*, α-PdH_x), but in contrast to the response case, the E_a measured for recovery did not vary with $[H_2]$ and it is impossible to determine whether H_2 desorption or the phase transition is rate-limiting since they have the same activation energy.[15] If, for α-PdH_x, H_2 adsorption and H_2 desorption are rate-limiting, then the rates of these processes should be directly proportional to the surface area/volume ratio (SA/*V*) of the sensing element.

Indeed, the response and recovery times are linearly correlated with the SA/*V* of the nanowires within the α-PdH_x regime (Figure 10). Plots of the response rate *versus* $\sqrt{[H_2]}$ (Figure 10a) and of the recovery rate *versus* $[H_2]$ (Figure 10b) are both linear for $[H_2] < 1\%$. The slopes of these plots can be used as a measure of the rates of these two processes for experiments that access the α-PdH_x. For the 12 devices probed above, the rates defined by these slopes are correlated with the SA/*V* (Figure 10c), but considerable scatter exists in these data, and particularly in the case of the response rate, it is clear that there are uncontrolled variables that influence the rate. The level of contamination of the nanowire surface, for example, is likely to be one of these variables.

All of the above data were acquired in a background of flowing N_2, and most actual hydrogen sensing is likely to occur in air. We carried out a comparison of the properties of two nanowires for detecting hydrogen in air and nitrogen backgrounds (Figure 11). The presence of the oxygen in air drives new reactions at the palladium surface that reduces the surface concentration of chemisorbed hydrogen, reducing slightly the amplitude of the resistance response (as originally observed by Hughes *et al.*[2]), and exerting a stronger influence on the rates of response and recovery. For a 25 × 85 nm palladium nanowire, the raw resistance *versus* time response to $[H_2]$ over the range from 0.2 to 1.0% (Figure 11a) shows the reduced sensitivity to H_2 in air *versus* N_2 and also the accelerated response and recovery times. The background resistance in the absence of H_2 is also lower by 8−9 kΩ, or 4.5%, in air as compared with N_2. A summary of $\Delta R/R_0$ *versus* $[H_2]$ (Figure 11b) reveals that no difference for $[H_2] > 4\%$, and a 8−12% reduction at lower concentrations. The LOD_{H_2} is increased from 2−5 ppm in N_2 to 1000−2000 ppm as a consequence of this reduced sensitivity in air. Recovery times were reduced by up to 40% for $[H_2] > 4\%$, and the acceleration effect is even stronger at lower H_2 concentrations (Figure 11d). Response times, on the other hand, were accelerated by up to a factor of 2 in the interval $2\% < [H_2] < 5\%$ but were virtually unaffected outside of this range. The pronounced influence of air on the rate of sensor recovery provides yet another indication that the kinetics of hydrogen desorption are rate-limiting for this process.

The depressed sensitivity for H_2 and the accelerated recovery rate seen in air are both understandable based upon the fact that the O_2 in air provides a new chan-

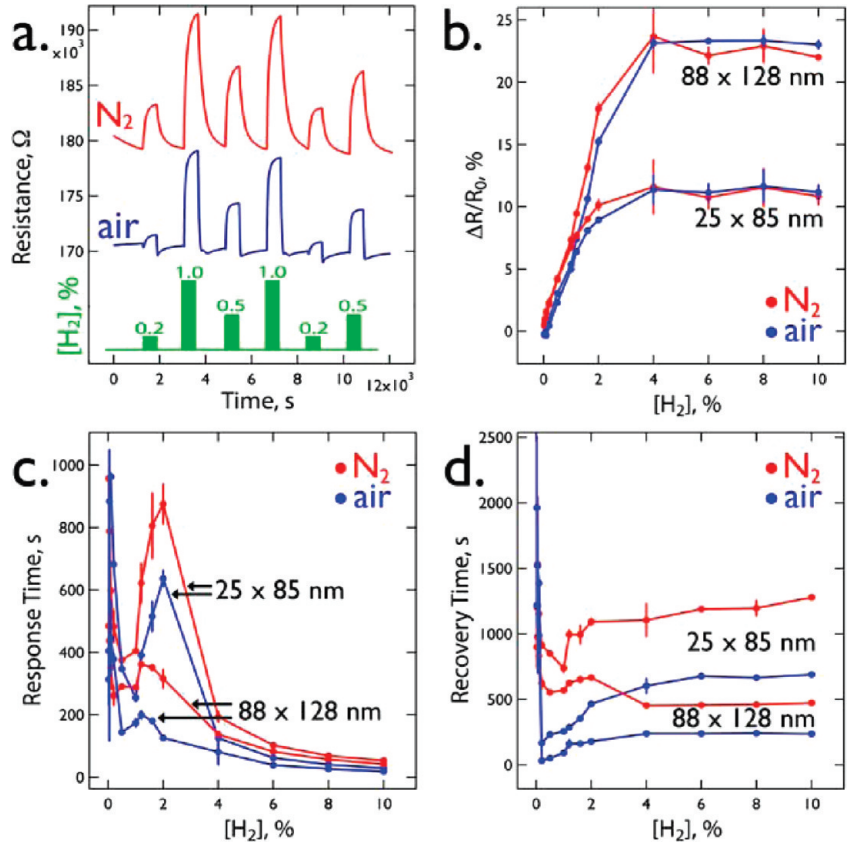

Figure 11. Hydrogen sensing in N_2 and in air for two nanowires. (a) Raw resistance *versus* time plots for the exposure of a 25 × 85 nm nanowire to hydrogen between 0.2 and 1.0%, as indicated at the bottom. (b) Calibration plots of $\Delta R/R_0$ *versus* $[H_2]$ for the same two nanowires shown in (a). (c) Plot of the response time *versus* $[H_2]$ for these two nanowires in air and N_2 as indicated. (d) Plot of the recovery time *versus* $[H_2]$ for these two nanowires in air and N_2 as indicated.

nel for the removal of chemisorbed hydrogen, H_a, from the palladium surface. This H_a removal process may occur, for example, by the reaction sequence proposed by Nyberg:[36]

$$O_2(gas) \rightarrow 2O_a \quad (5)$$

$$O_a + H_a \rightarrow (OH)_a \quad (6)$$

$$2(OH)_a \rightarrow O_a + (H_2O)_a \quad (7)$$

$$O_a + (H_2O)_a \rightarrow O_a + H_2O(gas) \quad (8)$$

The removal of H_a will reduce the equilibrium coverage of the palladium surface by H_a at every $[H_2]$, accounting for a reduction in the $\Delta R/R_0$ as seen in Figure 11b. The rate of hydrogen desorption in the absence of oxygen, $2H_a \rightarrow (H_2)_a \rightarrow H_2$, is augmented by reactions 5−8, readily explaining the acceleration of sensor recovery seen in air (Figure 11d).

The acceleration of sensor *response* in the concentration range just above the phase transition is not readily explained by this mechanism. It is apparent that the presence of adsorbed oxygen on the palladium surface modifies the kinetics of the phase transition, and this is an interesting and unexpected effect that warrants further study.

CONCLUSIONS

The main conclusions of this study are the following:

1. XPS depth profiling data show that "fracture-resistant" palladium nanowires[12] prepared by LPNE from EDTA-containing plating solutions do not contain excess bulk carbon. We conclude that the fracture toughness of these nanowires does not derive from a difference in composition for these nanowires, as compared with those prepared from EDTA-free solutions that *are* susceptible to fracture upon exposure to hydrogen.
2. Palladium nanowires and films both show $\Delta R/R_0 \propto \sqrt{P_{H_2}}$ below $[H_2] < 1\%$. Within this regime, smaller nanowires have a weakly enhanced sensitivity to hydrogen, but origin of this effect is not understood.
3. Palladium nanowires are significantly faster—both in terms of response and recovery—than palladium films having the same thickness. On the basis of this fact, a clear rationale exists for employing Pd nanowires as opposed to Pd films in these devices.
4. Smaller nanowires are faster hydrogen sensors than larger nanowires. The response and recovery rates observed for nanowires and films are approximately proportional to their surface area/volume ratio. This fact suggests that the rate-limiting processes in-

volved in response and recovery are surface-limited reactions, likely hydrogen adsorption and desorption. This conclusion is supported by our previous measurements of the activation energies associated with response and recovery.

5. Palladium nanowires have approximately the same sensitivity to H_2 in air as in N_2, but the absolute resistance change is reduced at all H_2 concentrations culminating in an increased LOD_{H_2} to 1000−2000 ppm from 2−5 ppm seen in N_2. Recovery times, on the other hand, are significantly reduced by factors of up to 100 for measurements carried out in an air background, and a slight decrease in response times are also observed in the $[H_2] = 2-5\%$ range.

METHODS

Chemicals. Optical glass slides (1 in. × 1 in.) were purchased from Fisher and used as substrates. Nickel wire (Ni, 99.99%) and palladium granule (Pd, 99.99%) were used as received from Aldrich. Positive photoresists S1808 and S1827 and developer F319 were purchased from Microchem. Palladium chloride ($PdCl_2$, 99.999%, certified ACS), potassium chloride (99.3%, certified ACS), EDTA (disodium ethylenediaminetetraacetate, 99.8%), and acetone (GR, ACS) were used as received from Fisher.

Nanowire Fabrication. The electrodeposition of palladium was carried out in a 50 mL, one-compartment, three-electrode cell. Pd nanowires were obtained from two different solutions, differentiated only by the presence of a slight stoichiometric excess of EDTA in one of them. The composition of the EDTA-containing solution was 0.1 M KCl, 0.2 mM $PdCl_2$, 0.22 mM EDTA (pH = 4.9), whereas the EDTA-free solution was identical except for the absence of added EDTA. Both plating solutions were prepared using Millipore Milli-Q water ($\rho \geq 18$ MΩ cm). Pd nanowire growth from the EDTA plating solution was carried out at −0.80 V *vs* SCE, whereas a potential of +0.18 V *vs* SCE was used in the EDTA-free solution. Nanowire deposition was controlled using a Gamry Instruments model G300 potentiostat/galvanostat.

XRD (X-ray Diffraction). GIXRD (grazing incidence X-ray diffraction)[37,38] technique was employed to analyze the crystallinity of Pd nanowires. A fixed, low angle of incidence for the X-ray beam makes the analysis more sensitive to the sample surface and thus leads to higher diffraction intensities. GIXRD was performed using a Rigaku Ultima III (Rigaku, Tokyo, Japan) high-resolution X-ray diffractometer with Cu Kα irradiation and an incident angle of 0.6°.

TEM (Transmission Electron Miscroscope) and SAED (Selective-Area Electron Diffraction). Linear Pd nanowires were first deposited onto glass by LPNE at either 5 or 2 μm interwire pitch. These nanowires were then released from the glass by etching in 2% HF solution for 5 min. A stream of water was then directed onto the glass surface, and the released Pd nanowires were washed onto carbon-coated copper grids (Ted Pella, Inc.) that were dried overnight before examination by TEM. Images and SAED measurements were obtained using a Philips CM20 TEM at an operating voltage of 200 KeV.

SEM (Scanning Electron Microscope). SEM images were collected on Philips XL-30 FEGSEM (field emission gun scanning electron microscope) using an accelerating voltage of 10 kV. The samples were mounted on aluminum stubs (Ted Pella) using adhesive carbon tape.

AFM (Atomic Force Microscope). Intermittent contact mode AFM images were acquired in air using an Asylum Research MFP-3D microscope and Olympus AC240TS tips.

XPS (X-ray Photoelectron Spectroscopy). XPS spectra were acquired with an ESCALAB MKII photoelectron spectrometer. The instrument is an ultrahigh vacuum system equipped with a Al/Mg twin anode X-ray source and a 150 mm hemispherical electron energy analyzer. Spectra were taken by using the Al Kα radiation (1486.6 eV), and the base pressure in the camber was 1×10^{-9} Torr throughout the experiment. The constant analyzer energy mode was used during the experiment, and constant pass energy for narrow scans was 20 eV. The photoelectron peaks of C1s and Pd3d were collected, and all peak positions were calibrated by using adventitious hydrocarbon at binding energy of 284.5 eV. Ar ion beam sputtering (2 keV) was used for depth profile analysis.

Hydrogen Sensing. H_2 sensors were prepared by evaporating a four-probe gold electrode of 60 nm thickness onto single, linear nanowires using a contact shadow mask. The four-contact electrical resistivity was measured using a source meter (Keithley Instruments, model 2400) in conjunction with a digital multimeter (Keithley Instruments, model 2000). Sensor measurements were carried out by placing the sensor in a sealed flow cell with a total dead volume of 120 μL. H_2 gas (Airgas, purity ≥99.998%) was premixed with N_2 (Airgas, purity ≥99.995%) to a predetermined concentration using flow controllers (MKS Inc., model 1479A), and pulses of this gas mixture were switched (Parker Valve, cycle time = 25 ms) into a steam of pure N_2 (Airgas, purity ≥99.995%) while maintaining a total flow rate of 1500 sccm. Instrument control and data acquisition were both coordinated by a computer equipped with Labview in conjunction with a National Instruments interface (model BNC 2110). All H_2 sensing measurements were carried out using dry gases at ambient laboratory temperature (≈20 °C) and atmospheric pressure.

Acknowledgment. This work was supported by the National Science Foundation (Grant CHE-0956524) and the UCI School of Physical Sciences Center for Solar Energy. J.C.H. and M.C. acknowledge funding from the DOE Office of Basic Energy Sciences (DE-FG02-96ER45576).

REFERENCES AND NOTES

1. Lewis, F. A. *The Palladium Hydrogen System*; Academic Press: London, 1967.
2. Hughes, R. C.; Schubert, W. K. Thin-Films of Pd/Ni Alloys for Detection of High Hydrogen Concentrations. *J. Appl. Phys.* **1992**, *71*, 542–544.
3. Funding Opportunity Announcement DE-PS36-09GO99004; Department of Energy Golden Field Office, Office of Energy Efficiency and Renewable Energy (EERE), 2009.
4. Rumiche, F.; Wang, H. H.; Hu, W. S.; Indacochea, J. E.; Wang, M. L. Anodized Aluminum Oxide (AAO) Nanowell Sensors for Hydrogen Detection. *Sens. Actuators, B* **2008**, *134*, 869–877.
5. DiMeo, J., Frank; Chen, I.-S.; Chen, P.; Neuner, J.; Roerhl, A.; Welch, J. MEMS-Based Hydrogen Gas Sensors. *Sens. Actuators, B* **2006**, *117*, 10–16.
6. Semancik, S.; Cavicchi, R.; Wheeler, M.; Tiffany, J.; Poirier, G.; Walton, R.; Suehle, J.; Panchapakesan, B.; DeVoe, D. Microhotplate Platforms for Chemical Sensor Research. *Sens. Actuators, B* **2001**, *77*, 579–591.
7. Kaltenpoth, G.; Schnabel, P.; Menke, E.; Walter, E.; Grunze, M.; Penner, R. Multimode Detection of Hydrogen Gas Using Palladium-Covered Silicon mu-Channels. *Anal. Chem.* **2003**, *75*, 4756–4765.
8. Xu, T.; Zach, M.; Xiao, Z.; Rosenmann, D.; Welp, U.; Kwok, W.; Crabtree, G. Self-Assembled Monolayer-Enhanced Hydrogen Sensing with Ultrathin Palladium Films. *Appl. Phys. Lett.* **2005**, *86*, 203104.
9. Ramanathan, M.; Skudlarek, G.; Wang, H. H.; Darling, S. B. Crossover Behavior in the Hydrogen Sensing Mechanism for Palladium Ultrathin Films. *Nanotechnology* **2010**, *21*, 125501.
10. Favier, F.; Walter, E.; Zach, M.; Benter, T.; Penner, R. Hydrogen Sensors and Switches from Electrodeposited Palladium Mesowire Arrays. *Science* **2001**, *293*, 2227–2231.
11. Kiefer, T.; Favier, F.; Vazquez-Mena, O.; Villanueva, G.;

Brugger, J. A Single Nanotrench in a Palladium Microwire for Hydrogen Detection. *Nanotechnology* **2008**, *19*, 125502.
12. Yang, F.; Taggart, D. K.; Penner, R. M. Fast, Sensitive Hydrogen Gas Detection Using Single Palladium Nanowires That Resist Fracture. *Nano Lett.* **2009**, *9*, 2177–2182.
13. Walter, E.; Favier, F.; Penner, R. Palladium Mesowire Arrays for Fast Hydrogen Sensors and Hydrogen-Actuated Switches. *Anal. Chem.* **2002**, *74*, 1546–1553.
14. Im, Y.; Lee, C.; Vasquez, R.; Bangar, M.; Myung, N.; Menke, E.; Penner, R.; Yun, M. Investigation of a Single Pd Nanowire for Use as a Hydrogen Sensor. *Small* **2006**, *2*, 356–358.
15. Yang, F.; Taggart, D.; Penner, R. Joule-Heating a Palladium Nanowire Sensor for Accelerated Response and Recovery to Hydrogen Gas. *Small* **2010**, *6*, 1422–1429.
16. Yun, M.; Myung, N.; Vasquez, R.; Lee, C.; Menke, E.; Penner, R. Electrochemically Grown Wires for Individually Addressable Sensor Arrays. *Nano Lett.* **2004**, *4*, 419–422.
17. Kim, K.; Sim, S.; Cho, S. Hydrogen Gas Sensor Using Pd Nanowires Electro-deposited into Anodized Alumina Template. *IEEE Sens. J.* **2006**, *6*, 509–513.
18. Jeon, K. J.; Jeun, M.; Lee, E.; Lee, J. M.; Lee, K.-I.; von Allmen, P.; Lee, W. Finite Size Effect on Hydrogen Gas Sensing Performance in Single Pd Nanowires. *Nanotechnology* **2008**, *19*, 495501.
19. Jeon, K. J.; Lee, J. M.; Lee, E.; Lee, W. Individual Pd Nanowire Hydrogen Sensors Fabricated by Electron-Beam Lithography. *Nanotechnology* **2009**, *20*, 135502.
20. Offermans, P.; Tong, H. D.; van Rijn, C. J. M.; Merken, P.; Brongersma, S. H.; Crego-Calama, M. Ultralow-Power Hydrogen Sensing with Single Palladium Nanowires. *Appl. Phys. Lett.* **2009**, *94*, 223110.
21. Menke, E. J.; Thompson, M. A.; Xiang, C.; Yang, L. C.; Penner, R. M. Lithographically Patterned Nanowire Electrodeposition. *Nat. Mater.* **2006**, *5*, 914–919.
22. Xiang, C.; Kung, S. C.; Taggart, D.; Yang, F.; Thompson, M. A.; Güell, A. G.; Yang, Y.; Penner, R. M. Lithographically Patterned Nanowire Electrodeposition: A Method for Patterning Electrically Continuous Metal Nanowires on Dielectrics. *ACS Nano* **2008**, *2*, 1939–1949.
23. Xiang, C.; Yang, Y.; Penner, R. M. Cheating the Diffraction Limit: Electrodeposited Nanowires Patterned by Photolithography. *Chem. Commun.* **2009**, 859–873.
24. Kabanov, S.; Perelygin, Y. Electrodeposition of Palladium–Zinc Alloy from the Ammonium Chloride-Na(2)EDTA Electrolyte. *Russ. J. Appl. Chem.* **2001**, *74*, 1958–1959.
25. de Oliveira, G.; Barbosa, L.; Broggi, R.; Carlos, I. Voltammetric Study of the Influence of EDTA on the Silver Electrodeposition and Morphological and Structural Characterization of Silver Films. *J. Electroanal. Chem.* **2005**, *578*, 151–158.
26. de Oliveira, G. M.; Carlos, I. A. Silver–Zinc Electrodeposition from a Thiourea Solution with Added EDTA or HEDTA. *Electrochim. Acta* **2009**, *54*, 2155–2163.
27. Moulder, J. F. *Handbook of X-ray Photoelectron Spectroscopy: A Reference Book of Standard Spectra for Identification*; Physical Electronics: Eden Prairie, MN, 1995.
28. Cabrera, A.; AguayoSoto, R. Hydrogen Absorption in Palladium Films Sensed by Changes in Their Resistivity. *Catal. Lett.* **1997**, *45*, 79–83.
29. Volkening, F.; Naidoo, M.; Candela, G.; Holtz, R.; Provenzano, V. Characterization of Nanocrystalline Palladium for Solid-State Gas Sensor Applications. *Nanostruct. Mater.* **1995**, *5*, 373–382.
30. Ward, T.; Dao, T. Model of Hydrogen Permeation Behavior in Palladium Membranes. *J. Membr. Sci.* **1999**, *153*, 211–231.
31. Bambakid, G.; Smith, R.; Otterson, D. Electrical Resistivity of the Palladium–Deuterium System. *Bull. Am. Phys. Soc.* **1968**, *13*, 957.
32. Smith, R.; Otterson, D. Electrical Resistivity of the PdH*x* System for H/Pd Atom Ratios to 0.97. *J. Phys. Chem. Solids* **1970**, *31*, 187.
33. Hughes, R. C.; Schubert, W. K.; Zipperian, T. E.; Rodriguez, J. L.; Plut, T. A. Thin-Film Palladium and Silver Alloys and Layers for Metal-Insulator-Semiconductor Sensors. *J. Appl. Phys.* **1987**, *62*, 1074–1083.
34. Kay, B.; Peden, C.; Goodman, D. Kinetics of Hydrogen Absorption by Pd(110). *Phys. Rev. B* **1986**, *34*, 817–821.
35. Mutschele, T.; Kirchheim, R. Segregation and Diffusion of Hydrogen in Grain-Boundaries of Palladium. *Scripta Metal* **1987**, *21*, 135–140.
36. Nyberg, C.; Tengstal, C. Adsorption and Reaction of Water, Oxygen, and Hydrogen on Pd(100)—Identification of Adsorbed Hydroxyl and Implications for the Catalytic H2–O2 Reaction. *J. Chem. Phys.* **1984**, *80*, 3463–3488.
37. Marra, W. C.; Eisenberger, P.; Cho, A. Y. X-ray-Total-External-Reflection-Bragg-Diffraction Structural Study of the GAAS-AL Interface. *J. Appl. Phys.* **1979**, *50*, 6927–6933.
38. Bontempi, E.; Colombi, P.; Depero, L.; Cartechini, L.; Presciutti, F.; Brunetti, B.; Sgamellotti, A. Glancing-Incidence X-ray Diffraction of Ag Nanoparticles in Gold Lustre Decoration of Italian Renaissance Pottery. *Appl. Phys. A: Mater. Sci. Process.* **2006**, *83*, 543–546.